

An Analysis of Polygenes Affecting Wing Shape on Chromosome 3 in *Drosophila melanogaster*

Kenneth Weber,* Robert Eisman,* Lisa Morey,* April Patty,*
Joshua Sparks,* Michele Tausek* and Zhao-Bang Zeng†

*Department of Biological Sciences, University of Southern Maine, Portland, Maine 04104-9300 and

†Department of Statistics, North Carolina State University, Raleigh, North Carolina 27695-8203

Manuscript received July 6, 1998

Accepted for publication June 8, 1999

ABSTRACT

Loci on the third chromosome of *Drosophila melanogaster* that affect an index of wing shape were mapped, using recombinant isogenic lines, with transposable elements as markers. Many genes with small subequal effects are dispersed along the whole chromosome. Their alleles act nearly additively in heterozygotes. They have small correlated effects on leg shape, but no detectable effects on halteres. Small negative net interactions occur over most of the chromosome. The data set of 519 recombinant isogenic lines can be explained reasonably well by two models. One model posits an indefinitely large number of loci with no interactions. The other model posits 11 loci with additive effects whose sum equals the total phenotypic range and with large positive and negative interactions that nearly cancel each other.

TWO recent studies of wing shape traits in *Drosophila melanogaster* have indicated a highly polygenic basis when shape is defined by metrics that remove the allometric effect of body size (Weber 1990, 1992). In the first study, wing-shape traits showed high realized heritabilities, symmetrical responses to divergent selection, and high ratios of long-term response to initial heritability (Weber 1990). These results show that many loci with small, localized effects on wing shape are segregating in the wild base population at intermediate frequencies. The second study showed that selection can change extremely small subregions of the wing while hardly affecting its major dimensions (Weber 1992). This adds to the evidence that wing shape is influenced by many commonly segregating loci with small and localized effects.

Here we advance to the next stage in the genetic analysis of wing shape—the attempt to map loci, estimate their magnitudes of effect, and describe their modes of action. Two strains of *D. melanogaster* with highly differentiated wing shapes were produced by selection for high and low values of a shape index. Isogenic crossing stocks were extracted, with third chromosomes high in one stock and low in the other, and with first and second chromosomes identical and low. Homozygous third-chromosome recombinants of these crossing stocks were analyzed using *in situ*-labeled transposable elements as markers. Recombination breakpoints were determined by comparison to the transposable element

insertion sites in the parent high and low third chromosomes. The pattern of wing phenotypes among recombinant lines yields a map of genetic effects along the chromosome (Long *et al.* 1995; Nuzhdin *et al.* 1997). Results are also presented here from crosses made to assess dominance and from measurements of the correlated effects of wing-shape genes on other appendages.

MATERIALS AND METHODS

The phenotypic scale: The trait in this study is trait F , defined in Weber (1990) as an index of wing shape incorporating two dimensions. The width of the wing across the middle is dimension D_1 , and the width across the base is dimension D_2 . On a scatterplot of D_1 vs. D_2 , each wing has some offset from a reference baseline. This offset is the phenotype, measured in radians as an angle of rotation about the origin. The reference baseline is empirically derived as a regression line through the scatterplot of D_1 vs. D_2 in a large sample of wild-type flies. The equation of the baseline is of the form $\theta = \beta r^\alpha$, derived by the regression of $\log(\theta)$ on $\log(r)$, after conversion of each point (D_1, D_2) to polar coordinates [where $\theta = \arctan(D_2/D_1)$ and $r = (D_1^2 + D_2^2)^{1/2}$; thus, $D_1 = r \cos \theta$ and $D_2 = r \sin \theta$]. Variations in the allometric relation of D_1 and D_2 are conveniently quantifiable as angular offsets from this baseline, *i.e.*, as an angle through which the baseline would have to be rotated about the origin to pass through any point (D_1, D_2). Points clockwise to the baseline are assigned a positive angular offset, points counterclockwise a negative angular offset, and points on the baseline have an offset phenotype of zero.

Angular offsets from control population baselines were also used to quantify correlated aspects of leg shape. Shape indexes for the femurs and tibiae of each leg were constructed by letting D_1 equal the widest distal width of each segment and D_2 the narrowest proximal width. Table 1 shows the empirical constants for the baseline equations of the control population for both wing- and leg-shape indexes, plus standard deviations of control population offsets from each baseline.

Corresponding author: K. Weber, Department of Biological Sciences, University of Southern Maine, Box 9300, Portland, ME 04104-9300. E-mail: keweber@usm.maine.edu

TABLE 1
Baseline constants from the control population

Shape trait	Exponent(α)	Coefficient(β)	SD
Wing width	-0.043	0.405	± 0.0063
Prothoracic femur width	-0.302	0.315	± 0.0153
Prothoracic tibia width	-0.217	0.270	± 0.0177
Mesothoracic femur width	-0.204	0.437	± 0.0178
Mesothoracic tibia width	-0.085	0.436	± 0.0206
Metathoracic femur width	-0.096	0.462	± 0.0195
Metathoracic tibia width	-0.177	0.320	± 0.0179

Constants in the formula for trait baselines ($\theta = \beta r^\alpha$) derived by regression from measurements of the control population. Each width trait is a shape trait based on two width dimensions. Standard deviations are in radians of angular offset of the control population around its own trait baselines.

Wing measurement: The "morphometer" system (Weber 1988) utilizes a small, hand-held suction device, attached to an air pump, to hold an anesthetized fly in a transparent frame that fits on the stage of a microprojector so that a large image of the wing can be focused on a digitizer pad. Wing landmarks are recorded as x and y pad coordinates. Measurements of wing dimensions obtained by this system have the same coefficients of variation as published measurements of wings that have been dissected and mounted on microscope slides (Cowley *et al.* 1986; Cowley and Atchley 1988; *cf.* Weber 1990, 1992). For each recombinant line, one right or left wing at random was measured from each of 50 male flies. The 50 males from each recombinant line were measured in two separate samples of 25, taken from two replicate culture vials, cultured on potato flake medium at 26°.

The crossing stocks: Starting from a large laboratory population that was founded from wild-caught flies, pairs of stocks with divergent wing shapes were created by 15 generations of mass selection of the extreme 20 individuals of 100 measured in each sex (Weber 1990). Five different angular-offset indexes of wing shape were used (designated as M , S , F , G , and R). After 3 yr in small vial cultures, the high F and low F lines were selected again for 5 more generations, then held in small vial cultures again for another 3 yr. Multiple isogenic lines were then extracted, and one high index- F line (HHH) and one low index- F line (LLL) with extreme phenotypes and excellent viability were chosen for mapping. From these stocks, three isogenic crossing stocks for the third chromosome were derived, with the three major chromosomes substituted as LLL, LLH, and LLB—where the letters L, H, and B indicate homozygous low index- F , homozygous high index- F , or balancer chromosomes, respectively. The balancer chromosomes used throughout this study were $FM7$ (with Bar) for chromosome 1, $SM5$ (with $Curly^P$)/ $Sternopleural$ for chromosome 2, and $TM6$ (with $Serrate$)/ $Stubble, brown^P$ for chromosome 3 (see Ashburner 1989). These stocks were all obtained from the Mid-America Drosophila Stock Center (Bowling Green, OH).

The markers: Insertion sites of the transposable element roo or $B104$ (Scherer *et al.* 1982; Lindsley and Zimm 1992, p. 1106) were labeled by a standard *in situ* protocol (*cf.* Long *et al.* 1995). The treatments (separated by appropriate transitional baths) were 20 min $2\times$ SSC at 65°, 3 min 0.14 M NaOH, air-drying, hybridization with biotinylated probe overnight, 20 min streptavidin/biotin treatment (Vectastain; Vector Laboratories, Burlingame, CA), 30 min in diaminobenzidine/ H_2O_2 solution, and light Giemsa counterstaining. The breakpoints for each recombinant line were confirmed by chromosome squashes of two larvae for every line. No recombinant lines

showed segregating *in situ* band patterns except for occasional single bands in new locations due to low-frequency spontaneous transpositions of roo .

The low third chromosome has insertions at 29 sites with 15 on the left arm and 14 on the right arm. The high third chromosome has insertions at 35 sites with 18 on the left arm and 17 on the right arm. These roo sites form rather complementary patterns, and only two or three markers are identical or ambiguous between high and low lines. Additional transposable elements 412 and 297 were used to resolve a gap in the distribution of roo sites on the right arm. The extra bands located with these markers were at 90D1, 90E3, and 91D1. In all, 62 markers were located at sufficiently differentiable positions to be easily referable to one line or the other in recombinants. Thus each useful marker represents on average $111/62 = 1.8$ cM. Table 2 shows the cytological positions of all 62 useful markers, with estimated genetic distances in centimorgans from the left end. Distances were estimated from a graph of centimorgans as a function of band location, based on the tables of gene locations by Ashburner in Lindsley and Zimm (1992, p. 1117). The first three markers on the left tip of the chromosome are not separable on the linkage map.

Crossover breakpoint mapping: The crossing stocks were used to produce recombinant third chromosomes by crossing LLL \times LLH to create females heterozygous for the third chromosome, crossing these to males of the LLB balancer stock, and crossing the male progeny of these back to the balancer stock again, to extract isogenic lines with L \times H recombinant third chromosomes. Also at one point a L-H single-recombinant line with breakpoint at 67F1-69A1 was crossed to an H nonrecombinant line to gain resolution on the left arm. This produced a total of 34 L-H single recombinants with breakpoints left of 67F1-69A1, and 23 H-L-H double recombinants with a second breakpoint at 67F1-69A1. In the recombinant isogenic lines, the X and the second chromosome are isogenic among all lines, the Y chromosome must always be from the original low line, and the fourth chromosomes could be from the parent high, low, or original balancer stocks. The fourth chromosome carries $\sim 1\%$ of the euchromatic genome (Hartl and Lozovskaya 1995) and thus can be ignored.

Measurement of correlated effects on appendages: Legs of lines LLH and LLL and of control lines were mounted on slides in glycerol under coverslips sealed with fingernail polish. Left legs were positioned with anterior side upward and partly flexed femorotibial joint. Leg images were projected from the slides and measured in the same way as wings. Comparisons

TABLE 2
Positions of transposable element markers

Band	Chromosome	Centimorgans	Band	Chromosome	Centimorgans	Band ^a	Chromosome	Centimorgans
61A1	H	0.0	70F3	L	41.1	88D6	L	53.7
61D1	H	0.0	70F7	H	41.5	88D8	H	54.2
61E2	H	0.0	72A1	H	43.3	89A1	L	56.3
61F3	L	0.1	75B5	L	45.3	90D1	H	61.0
62B1	L	1.3	75C3	H	45.4	90E3	H	62.0
62B7	H	1.4	75E1	L	45.6	91D1	H	64.3
62D1	H	1.5	75F6	L	45.7	92D1	L	66.9
62D5	H	1.6	76F1	H	46.0	93E4	H	72.0
62E6	H	2.3	77C1	H	46.1	94D1	H	76.1
63E1	H	6.2	78A1	L	46.3	94F1	H	78.0
63E6	L	6.8	78C1	H	46.4	96A1	H	84.0
64B12	H	12.7	82A1	H	46.9	96D2	H	89.6
64D1	L	17.4	82B1	L	47.0	97C3	H	91.3
64D3	L	18.4	82C1	L	47.1	98A5	H	96.1
64E1	L	19.2	83A1	L	47.2	98A7	H	97.0
65B1	H	20.9	83E1	H	47.3	99F10	H	101.7
65D3	H	21.7	84A1	L	47.4	100B1	L	103.0
66C3	H	25.9	84D6	L	47.5	100B4	L	104.3
67F1	L	33.8	85F7	L	48.5	100C1	L	105.5
69A1	L	37.8	86B6	H	49.0	100F1	H	109.1
69A2	L	38.0	87A1	H	50.8			

Locations of 62 distinguishable marker sites in high (H) and low (L) third chromosomes.

^aAll are *roo* insertions except for three sites of transposable elements 412 (90D1, 91D1) and 297 (90E3).

between LLH and LLL leg shapes were made in terms of their angular offsets from control population baselines for femurs and tibiae of prothoracic, mesothoracic, and metathoracic legs.

Detached and mounted halteres cannot be measured with precision, being compressible and round with no reproducible plane of mounting. For this reason it was necessary to measure unmounted halteres still attached to live anesthetized flies. All were measured with bodies positioned in the morphometer in the same viewing plane. Halteres were not compared by their offsets from control baselines; instead dimensions of LLL and LLH halteres were compared directly. This removed the necessity of also measuring a large sample of control halteres. To avoid body-size complications in haltere measurements, flies of the LLH and LLL lines were cultured at similar density and matched carefully for body size.

Statistical separation of chromosome regions: To estimate the minimum number of segments with effects on the trait, the data set was first simplified by excluding all lines except (1) single-recombinant lines at breakpoints having at least four lines in both the HL and LH directions and (2) the H and L nonrecombinant lines. Starting from the left end of the chromosome, single-recombinant means at successive breakpoints were compared to the left-end nonrecombinant mean until the combined probability of the two phenotypic differences (HL – L, and LH – H) reached $P < 0.01$. Starting at this breakpoint, the same procedure was applied again until the whole chromosome was separated into significantly different intervals.

Individual and combined probabilities per interval were calculated as follows. The probability of the individual phenotypic difference at each interval was first evaluated for each direction (HL or LH) with a *t*-test based on the means and variances of line means at each breakpoint. Only phenotypic differences in the same direction as the total chromosome (HL or LH) were considered, thus all *t*-tests were one-tailed. Exact probabilities for each *t*-test were calculated using a com-

puter program (K.W.) of the series expansions given in Abramowitz and Stegun (1970, p. 948, items 26.7.3 and 26.7.4), which exactly reproduces all tabulated *t*-test probabilities across the whole experimental range. The separate *t*-test probabilities for each direction (HL or LH) were then combined for each interval by calculating for each pair of probabilities the sum $-\Sigma \ln(P)$, which is distributed as chi-square with $2k$ d.f., where k is the number of separate tests (Sokal and Rohlf 1969, p. 623). Combined probability thresholds for each interval were then taken from a standard table of chi-square values using 4 d.f.

Multiple interval mapping analysis: Quantitative trait loci (QTL) analysis was performed using the multiple interval mapping (MIM) method of Kao *et al.* (1999). This is a multiple QTL-oriented method that combines QTL mapping with analysis of genetic architecture through maximum-likelihood analysis and a search algorithm to determine number, positions, effects, and interactions of significant QTL. The model of multiple interval mapping for m QTL is specified as

$$y_i = \mu + \sum_{r=1}^m \alpha_r x_{ir}^* + \sum_{r \neq s \subset (1, \dots, m)} \beta_{rs} (x_{ir}^* x_{is}^*) + e_i$$

where y_i is the phenotypic value of individual i ; μ is the mean of the model; α is the marginal effect of putative QTL r ; x_{ir}^* is an indicator variable denoting genotype of putative QTL r (defined by $1/2$ or $-1/2$ for the two genotypes), which is unobserved but can be inferred from the marker data; β_{rs} is the epistatic effect between putative QTL r and s ; $r \neq s \subset (1, \dots, m)$ denotes a subset of QTL pairs that shows a significant epistatic effect (because if all pairs of m QTL are fitted in the model, the model can be overparameterized); m is the number of putative QTL chosen on the basis of either their significant marginal effects or significant epistatic effects; and e_i is a residual effect of the model assumed to be normally distributed with mean zero and variance σ^2 .

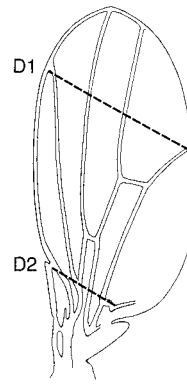
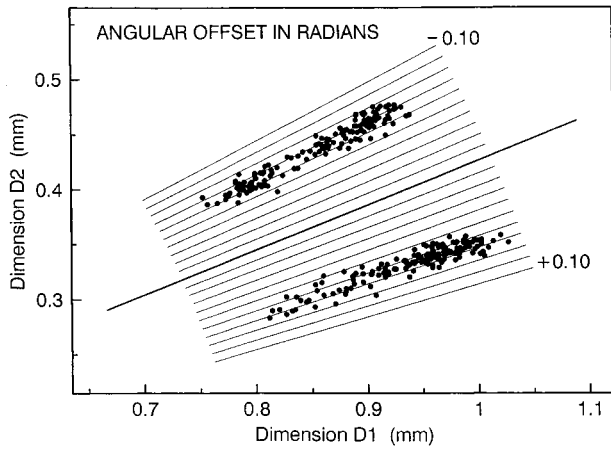


Figure 1.—Scatterplots of isogenic parent lines HHH and LLL, showing the scale of angular offset calibrated in intervals of 0.01 rad. The mean offsets of the two samples are $\sim +0.065$ rad for HHH and ~ -0.065 rad for LLL ($N = 150$). The central baseline is the line of allometry of D_1 and D_2 in base population flies (polar equation, $\theta = 0.4048r^{-0.043}$) derived by regressing $\log(\theta)$ on $\log(r)$.

The likelihood function of the data is

$$L(\mathbf{E}, \mu, \sigma^2) = \prod_{i=1}^n \left[\sum_{j=1}^{2^m} p_{ij} \phi(y_i | \mu + \mathbf{D}_{ij}\mathbf{E}, \sigma^2) \right],$$

where p_{ij} is the probability of each multilocus QTL genotype conditional on marker data; \mathbf{E} is a vector of QTL parameters (α 's and β 's); \mathbf{D}_{ij} is a vector of the genetic model design specifying the configuration of x^* 's associated with each α and β for the j th QTL genotype (Kao and Zeng 1997; Kao *et al.* 1999); and $\phi(y^* | \mu, \sigma^2)$ denotes a normal density function for y with mean μ and variance σ^2 . The bracketed term is a weighted sum of a series of normal density functions, one for each of 2^m possible multiple-QTL genotypes. Although the number of possible mixture components (QTL genotypes) increases exponentially with the number of QTL and can be very large when m is not small, the number of QTL genotypes that have appreciable probabilities given marker genotypes, and that contribute nontrivially to likelihood analysis, may not be large.

Analysis of likelihood is by an EM algorithm (Kao and Zeng 1997). The test for each QTL effect is performed by a likelihood ratio (in LOD) conditional on other selected QTL effects. For testing a null hypothesis of $H_0: E_r = 0$ against $H_1: E_r \neq 0$, $\text{LOD} = \log_{10}[L_1(E_r \neq 0)/L_0(E_r = 0)]$, where L_0 and L_1 are maximum likelihoods under H_0 and H_1 , respectively, conditional on all other selected QTL effects.

A search for genetic models for likelihood evaluation was performed in two steps. First, several simplified procedures were used (see below) to select a premodel, to reduce the numerical burden of MIM analysis in model selection, and to combine information from different analyses to arrive at an appropriate starting model.

Given an initial model, the following stepwise selection analysis was performed to finalize the search for a genetic model under MIM:

1. Begin with a model that contains m QTL and t epistatic effects.
2. Scan the genome to search for the best position of an $(m + 1)$ th QTL, and then perform a likelihood-ratio test for the marginal effect (α_{m+1}) of this putative QTL. If the test statistic exceeds the critical value (see below), α_{m+1} is retained in the model.
3. Search for the $(t + 1)$ th epistatic effect (β_{t+1}) among those pairwise interaction terms not yet included in the model, and perform the likelihood ratio test on β_{t+1} . If LOD exceeds the critical value (see below), β_{t+1} is retained in the model. Repeat the process until no more significant epistatic effects are found.

4. Reevaluate the significance of each QTL effect currently fitted in the model. If LOD for a marginal or epistatic effect falls below the significance threshold conditional on other fitted effects, the effect is removed from the model. However, if the marginal effect of a QTL that has significant epistatic effect with other QTL falls below the threshold, this marginal effect is still retained. This process is repeated until the test statistic for each effect is above the significance threshold.
5. Optimize estimates of QTL positions based on the currently selected model. Instead of performing a multidimensional search around the regions of current estimates of QTL positions (which is an option), estimates of QTL positions are updated in turn for each region. For the i th QTL in the model, the region between its two neighbor QTL is scanned to find the position that maximizes the likelihood (conditional on the current estimates of positions of other QTL and QTL epistasis). This refinement process is repeated sequentially for each QTL position until there is no change in estimates of QTL positions.
6. Return to step 2 and repeat the process until no more significant QTL effect can be added into the model and estimates of QTL positions are optimized.

It is not clear how to determine an appropriate stopping rule for this method, with multiple locus main effects and epistatic effects combined in a single model. For this analysis, $\text{LOD} = 2$ was adopted as the critical value for retaining a QTL effect in the model. Permutation resampling was performed (Churchill and Doerge 1994) at the request of a reviewer, and a 5% permutation threshold of $\text{LOD} = 1.89$ was obtained for the data set. However, it should be pointed out that this permutation threshold, simulated at the null hypothesis of no QTL, is suited for the test of zero vs. one QTL and does not address the issue of model selection.

The analysis with $\text{LOD} = 2$ threshold picked up 10 QTL. The next putative QTL has the support of $\text{LOD} = 1.2$ and has a negative effect. Considering the strong appearance of repulsion linkage at this site in the raw data shown in Figure 2, we decided to retain this QTL in the model and correspondingly lowered the threshold for admitting epistatic effects to $\text{LOD} = 1$ for the purpose of estimating the relative contribution of epistatic effects to the total variance, as there are not many very significant QTL epistatic effects on the trait.

Given a selected model that contains the number and positions of QTL and QTL pairs interacting significantly, the estimation of QTL effects and the variance explained by selected QTL effects can be obtained from the likelihood analysis. This explained variance, σ_g^2 , can be further partitioned into individual variances and covariances of QTL effects as

$$\hat{\sigma}_g^2 = \sum_{r=1}^{m+t} \left[\frac{1}{n} \sum_{i=1}^n \sum_{j=1}^{2m} \hat{\pi}_{ij} (D_{ijr} - \bar{D}_r)^2 \hat{E}_r^2 \right] + \sum_{r=2}^{m+t} \sum_{s=1}^{r-1} \left[\frac{2}{n} \sum_{i=1}^n \sum_{j=1}^{2m} \hat{\pi}_{ij} (D_{ijr} - \bar{D}_r) (D_{ijs} - \bar{D}_s) \hat{E}_r \hat{E}_s \right] = \sum_{r=1}^{m+t} \hat{\sigma}_{E_r}^2 + \sum_{r=2, s=1}^{m+t, r-1} \hat{\sigma}_{E_r, E_s}$$

with $\bar{D}_r = \sum_{i=1}^n \sum_{j=1}^{2m} \hat{\pi}_{ij} D_{ijr} / n$ and

$$\pi_{ij} = \frac{p_j \phi(y_i | \mu + \mathbf{D}_{ij} \mathbf{E}, \sigma^2)}{\sum_{j=1}^{2m} p_j \phi(y_i | \mu + \mathbf{D}_{ij} \mathbf{E}, \sigma^2)}$$

This can be derived from the maximum-likelihood estimate of residual variance (Kao and Zeng 1997). Here, π_{ij} is the probability of each multilocus QTL genotype conditional on marker genotype and also phenotypic value. In this formulation, $\hat{\sigma}_{E_r}^2$ estimates genetic variance due to QTL effect E_r and $\hat{\sigma}_{E_r, E_s}$ estimates genetic covariance between QTL effects E_r and E_s .

RESULTS

Figure 1 shows the index F baseline and samples of the isogenic parent lines. In one sample all three main chromosomes are high (HHH) and the angular offset is clockwise; in the other sample all three are low (LLL) and the offset is counterclockwise. The mean offsets of these lines differ by ~ 0.13 rad, or 20 standard deviations of the base population. The figure illustrates three important facts about the trait. First, in the range of body size of these studies, wing shape is essentially independent of size when quantified by offsets from natural baselines. Second, the phenotypic correlation of D_1 and D_2 is extremely positive even though selection makes both dimensions change in a negatively correlated way. Third, selection on angular offset in wings causes an orderly rotation of the baseline about the origin, not a random realignment of the long axis.

The mean offset of 15 nonrecombinant L third-chromosome lines (LLL) derived from these crosses was -0.0689 rad, and the mean of 15 nonrecombinant H third-chromosome lines (LLH) was -0.0073 rad. The phenotypic difference of 0.0616 radians is the total effect of the third chromosome mapped in this study. In all, 519 lines were measured, or 25,950 wings. The third chromosomes of measured lines included 194 L-H single crossovers, 149 H-L single crossovers, 70 H-L-H double crossovers, 58 L-H-L double crossovers, 7 H-L-H-L triple crossovers, 11 L-H-L-H triple crossovers, 15 H nonrecombinants, and 15 L nonrecombinants. (Many more nonrecombinant lines were found but not measured.)

Single-recombinant lines: Figure 2 shows the phenotypes of single-recombinant lines as a function of recombination breakpoint. The profiles show clearly the cumulative effect of short sequentially added chromosome segments, starting from either a low or a high nonrecombinant chromosome. Effects occur all along the chromosome, and there is a strong appearance of repul-

sion linkage in one or more regions where the profiles are nonmonotonic, for example, between 70 and 90 cM. The graphs of single-recombinant phenotypes convey, without further analysis, several of the most interesting qualitative results of this study. Many intervals along the third chromosome show discernible effects on the shape index, indicating genes located diffusely along most of the chromosome. The effects do not appear to fall into distinct categories of major and minor, and compared to the wing as a whole the effects are all very small.

The minimum number of genes: In analyses of QTL, minor QTL may crop up that are only statistical artifacts, especially if a large number of QTL are claimed. With the present large data set, one can get a preliminary idea of the distribution of effects along the chromosome by differentiating segments with a series of t -tests, using the single-recombinant data of Figure 2. Only breakpoints with four or more lines in both directions (LH

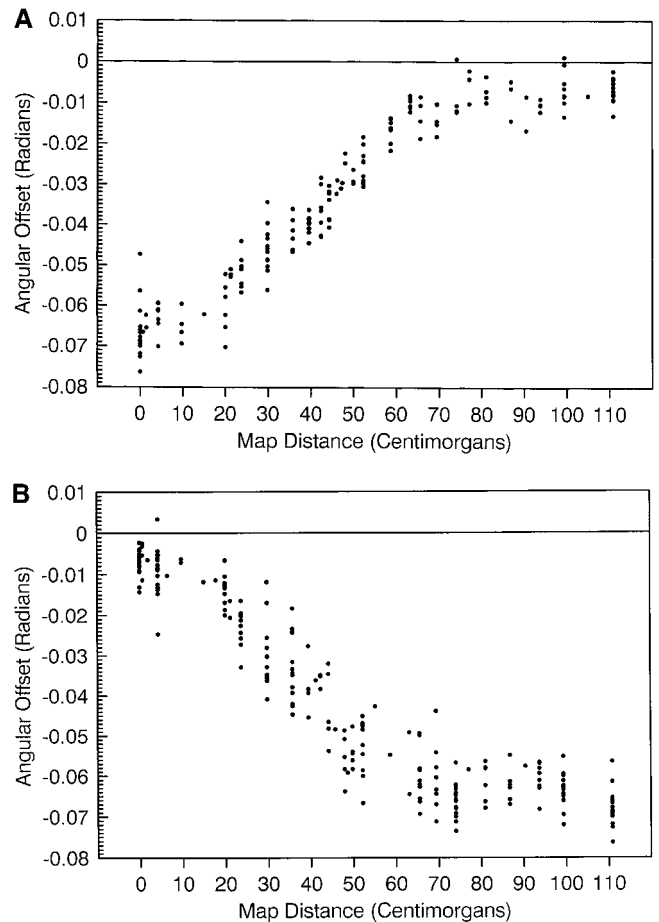


Figure 2.—Phenotypes of single-recombinant lines as a function of recombination breakpoint. Breakpoints are estimated as midpoints between adjacent marker sites. Centimorgan values are estimated from band locations. Points at ends are samples of 15 H or L nonrecombinant lines. (A) High-low lines of chromosome 3. Phenotypes of 149 HL single recombinants plus nonrecombinants. (B) Low-high lines of chromosome 3. Phenotypes of 194 LH single recombinants plus nonrecombinants.

TABLE 3
Division of chromosome 3 into eight segments

Centimorgans	HL lines			LH lines			Segment	Effect	<i>P</i>
	<i>n</i>	Mean	SD	<i>n</i>	Mean	SD			
0.0	15	-0.0689	±0.0047	15	-0.0073	±0.0033	1	0.0042	<0.01
4.3	7	-0.0628	±0.0037	18	-0.0095	±0.0060	2	0.0125	<0.0001
23.8	8	-0.0514	±0.0041	11	-0.0231	±0.0045	3	0.0061	<0.005
29.9	12	-0.0461	±0.0057	12	-0.0299	±0.0084	4	0.0068	<0.005
39.6	8	-0.0400	±0.0025	5	-0.0374	±0.0064	5	0.0052	<0.01
44.3	7	-0.0352	±0.0041	5	-0.0430	±0.0093	6	0.0099	<0.001
52.3	13	-0.0258	±0.0040	9	-0.0534	±0.0072	7	0.0110	<0.001
65.6	4	-0.0107	±0.0076	12	-0.0602	±0.0065	8	0.0061	<0.001
110.9	15	-0.0073	±0.0033	15	-0.0689	±0.0047			

Analysis of chromosome 3 by serial *t*-tests with combined $P < 0.01$. Only significantly different (segment-defining) breakpoints are given, with location (cM), number of lines (*n*), and phenotypic mean ±SD. For each numbered segment, effect is mean of phenotypic differences in both LH and HL directions; effects must total ~0.0616 rad. Combined probabilities (*P*) were calculated as explained in materials and methods.

and HL) were considered. Starting at the left end of the chromosome and moving right, the mean at each breakpoint was compared to the left-end mean until reaching a breakpoint where the difference, in both the HL and LH directions, attained a combined significance of $P < 0.01$ (see materials and methods). This defined the first segment with significant effect. Continuing from this point, a second breakpoint was reached, where the difference from the last starting point again reached a combined significance of $P < 0.01$. The objective was not to assess each fluctuation that might be due to a gene, but to estimate the minimum number of segments contributing to the total phenotypic difference of 0.0616 rad. Thus only differences in the overall forward direction were considered. Proceeding to the right end of the chromosome, this method separates it into eight segments (Table 3). This analysis does not incorporate the information available from the 146 multirecombinant lines or the 212 single-recombinant lines at intermediate or excluded breakpoints. This is, however, enough to show that at least eight loci contribute effects.

Independent gene action *vs.* interaction: The profiles of HL and LH single-recombinant means are nearly the same when one is inverted on the other (Figure 3A). This shows that the effects of individual loci are not much different whether they are sequentially combined from left to right or from right to left. Figure 3B shows the weighted mean of the two graphs in Figure 3A for all breakpoints with two or more single recombinants

in both directions (there are 21 such breakpoints). This shows the cumulative mean genetic effect of short segments.

Wherever two loci interact, the profiles in Figure 3A must be separated between the sites involved by a distance equal to the magnitude of the interaction. If multiple pairwise interactions exist, the sites involved may be arranged in various patterns, overlapping each other, embedded, or end-to-end, and only the net interaction across each breakpoint would be revealed in Figure 3A. Figure 3C shows the difference between the HL and LH means in Figure 3A for breakpoints with two or more single recombinants in both directions. This estimates graphically the magnitude and sign of the net interaction between loci to the left and right of each point. Interactions across the central region of the chromosome have a net positive effect; the net effect along the arms is negative. These could represent many small local interactions, or a few small widely separated interactions, or strong overlapping interactions that cancel each other. This also does not rule out strong interactions between closely linked loci that did not recombine nor interactions with loci on other chromosomes.

A model with many independently acting polygenes: If one assumes an indefinitely large number of loci, all acting independently (additively), Figure 3B becomes a model that can be used to predict the phenotype of any recombinant line. If the breakpoints of a chromosome are projected upward to intersect the graph, the predicted effect of each L or H segment can be read

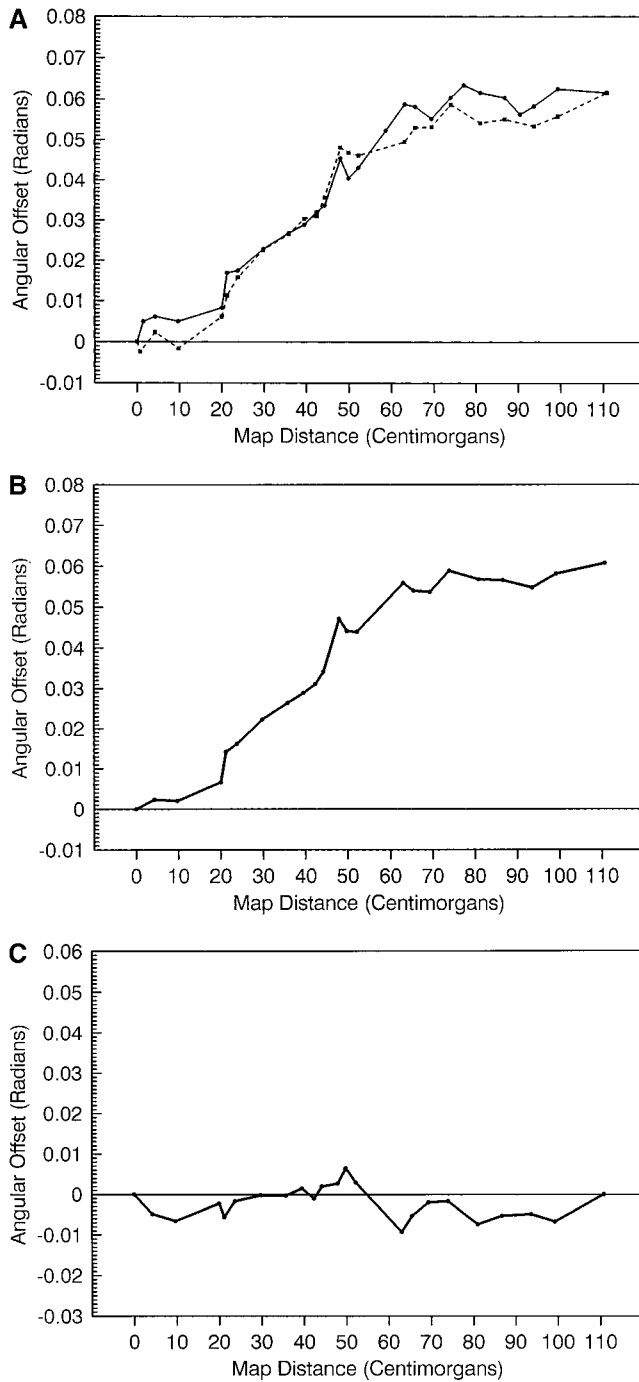


Figure 3.—(A) Mean effects in both directions. Comparison of mean profiles of Figures 2A (solid line) and 2B (dashed line), with 2B inverted. The mean of each point cluster is plotted as a positive difference from the left-end mean of non-recombinants. All breakpoints with ≥ 2 recombinant lines are included. (B) Cumulative mean effect. Graph of weighted average effect of single recombinants of both types for breakpoints with ≥ 2 recombinant lines in both directions. (C) Net interactive effects by region. Graph of LH - HL (from A) for breakpoints with ≥ 2 recombinant lines in both directions.

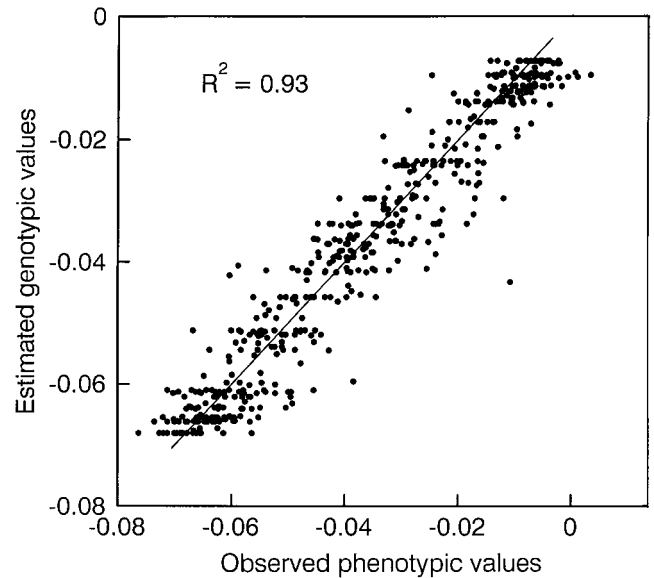


Figure 4.—Comparison of the observed phenotypes of all 519 measured lines (zero, one, two, or three breakpoints), with their phenotypes as predicted by the graph of single-recombinant means (Figure 3B). Predicted phenotypes were interpolated from the graph according to recombination breakpoints by a computer program.

off on the y -axis. A computer program was written to estimate the phenotype of any recombinant line by interpolation from Figure 3B. This simple model is reasonably successful in explaining the phenotypic variation of the whole data set, with an R^2 of 0.93 (Figure 4).

The model can also be checked by considering the variance within each recombinant category along with its necessary increase in error. The error variance must increase with each additional breakpoint among single-, double-, and triple-recombinant lines, because when a gene for the trait falls in any interval, crossovers can be either right or left of it. The mean increase in error variance among line means per breakpoint can be estimated empirically from the difference between single recombinants and nonrecombinants. Thus the variance among nonrecombinant lines of identical *roo* genotype (mean of S_H^2 and S_L^2 , total of 30 lines) is 0.000016; and the variance among single-recombinant lines of identical *roo* genotype (weighted mean variance of line means at 22 HL and 21 LH breakpoints having >2 lines, total of 314 lines) is 0.000029; the difference is +0.000013 or the effect of one breakpoint. Therefore the mean variance among line means of identical *roo* genotype in any recombinant class, equal to the error variance among line means for the whole recombinant class, can be estimated as 0.000016 plus 0.000013 times the number of breakpoints. The resulting estimates of total phenotypic variance are compared with observed phenotypic variance in each recombinant class in Table 4 and Figure 5.

Results of multiple interval mapping: Several analyses

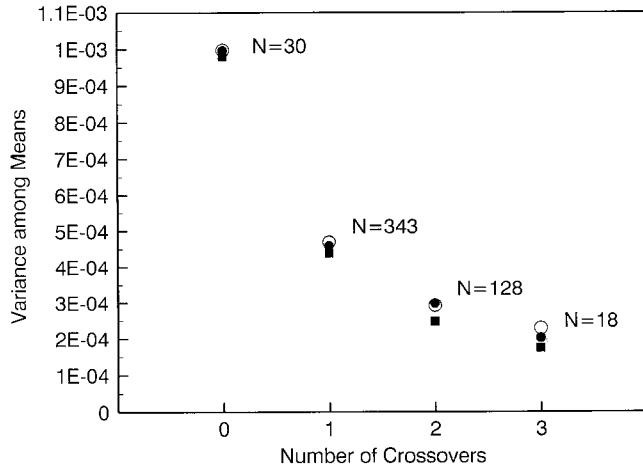


Figure 5.—Variances among all nonrecombinant lines (L and H), all single recombinant lines (LH and HL), all double recombinant lines (LHL and HLH), and all triple recombinant lines (LHLH and HLHL). ●, observed phenotypic variance among line means; ■, variance among line means predicted from Figure 3B; ○, sums of predicted variance and estimated error variance. Data are from Table 4.

were first performed to select a premodel for MIM analysis. The first analysis was a backward stepwise regression analysis on markers based on F -to-drop statistic with $\alpha = 0.01$. This analysis selected 10 markers, with $R^2 = 0.93$. The second analysis was by composite interval mapping (Zeng 1994) using QTL Cartographer (Basten *et al.* 1998). The markers selected by backward stepwise regression were used as background markers in model 6 of QTL Cartographer with a window size of 3 cM (after trying a few other values). This analysis identified 10 significant positions based on a LOD = 2 criterion. The positions identified here, though generally agreeing with those marker positions picked by backward stepwise regression, differ significantly in a few critical major regions.

Based on these analyses, a premodel of 10 putative QTL positions was selected for MIM analysis, and the search process was started using the stepwise selection procedure. After several cycles of adding, dropping, and optimizing, the model quickly stabilized at 10 QTL and

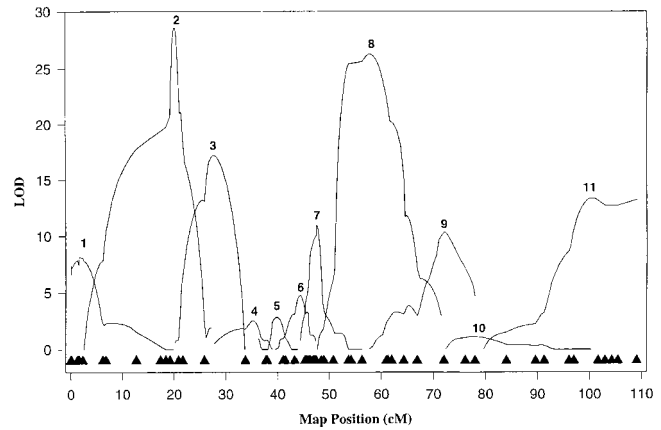


Figure 6.—Marginal likelihood profiles of 11 QTL identified by multiple interval mapping. LOD score as a function of genetic map location. The likelihood profile for each QTL extends from near the estimated position of one neighbor QTL to the other or to the end of the chromosome. Triangles indicate marker positions.

5 significant epistatic effects, based on the LOD = 2 criterion. Given this model, the next QTL that may be considered is the one near 78 cM, showing repulsion linkage with other QTL. Although the support for this QTL (LOD = 1.2) is below the subscribed threshold, there is enough evidence from Figure 2 to include this QTL in the model. Subsequently, the threshold for epistatic effects was also lowered to LOD = 1, and 4 more epistatic effects were picked up. The final model contains 11 QTL main effects and 9 epistatic effects, with $R^2 = 0.96$.

A search was made for significant epistatic effects between selected QTL positions and unselected positions to identify potential QTL that show significant epistatic effects but not significant marginal effects. This was done in a stepwise manner by seeking the largest epistatic effect between a given QTL position and an unselected position at 1-cM intervals and testing it for significance. However, the current model fits the data very well, and hardly any new component can improve the fit. This is not to say that no potential candidate pairs can be picked up. When they are picked up, the

TABLE 4
Observed and predicted variances by recombinant category

	Nonrecombinant	Single	Double	Triple
Variances of predicted means	0.000981	0.000439	0.000248	0.000174
Estimated error variances	0.000016 ^a	0.000029 ^a	0.000042 ^b	0.000055 ^b
Totals	0.000997	0.000468	0.000290	0.000229
Variances of observed means	0.000997	0.000459	0.000298	0.000202

Variances among line means, as predicted by model of unlimited polygenes with no interaction, plus estimated error variances among line means, compared to observed variances among line means.

^aEmpirical mean values.

^bExtrapolated values.

TABLE 7

Estimated variances and covariances of QTL epistatic effects in ratio of total phenotypic variance

QTL pair	(1, 2)	(2, 4)	(3, 8)	(3, 9)	(4, 5)	(5, 8)	(5, 9)	(6, 10)	(8, 11)	Sum
(1,2)	0.001	0.000	0.000	0.001	0.000	0.000	-0.001	0.000	0.000	0.001
(2,4)	0.000	0.001	0.000	0.000	0.000	0.001	-0.001	0.000	0.000	0.001
(3,8)	0.000	0.000	0.009	-0.011	0.001	-0.005	0.004	0.000	-0.001	-0.004
(3,9)	0.001	0.000	-0.011	0.027	-0.001	0.005	-0.014	0.002	0.001	0.009
(4,5)	0.000	0.000	0.001	-0.001	0.002	0.000	-0.001	0.000	0.000	0.001
(5,8)	0.000	0.001	-0.005	0.005	0.000	0.008	-0.008	0.001	0.001	0.004
(5,9)	-0.001	-0.001	0.004	-0.014	-0.001	-0.008	0.021	-0.003	0.000	-0.003
(6,10)	0.000	0.000	0.000	0.002	0.000	0.001	-0.003	0.001	-0.001	0.001
(8,11)	0.000	0.000	-0.001	0.001	0.000	0.001	0.000	-0.001	0.003	0.002
Total										0.012

stocks were crossed either to a nonrecombinant isogenic high third-chromosome (LLH) stock or to a nonrecombinant isogenic low (LLL) stock, according to the scheme in Figure 7. Hybrid lines created in this way are homozygous L or H for the whole chromosome segment on one side of the breakpoint and heterozygous on the other side. The phenotypes of these hybrid lines were mostly near the midpoint between the parental phenotypes, showing near additivity of alleles in the heterozygous part. In every cross there was a slight dominance of H alleles, which in this case means dominance in the direction of the wild-type phenotype. This pattern is consistent across the whole chromosome in either direction of the crossing scheme.

Correlated effects on leg shapes: The leg shapes of LLH and LLL flies cultured under identical conditions were compared to test the third chromosome as a whole for correlated effects of wing-shape genes. Leg-shape indexes were constructed for the femur and the tibia, the two main leg segments. D_1 was the widest part of each segment and D_2 was the narrowest (and more proximal) part of the same segment, so these shape indexes were somewhat analogous to the one used for the wing. Baselines for these indexes were derived from measurements of control flies, and the angular offsets of LLH and LLL flies from these baselines were then compared with each other exactly as in the wing measurements. In all three legs, the differences between LLH and LLL are always negative for the femur and positive for the tibia (Table 8). These differences are also all highly significant ($P < 10^{-6}$). However, they are small compared to the difference in wing shape. The mean leg-shape difference is only 1.29 SD of the base population, while the wing-shape difference is 9.78 SD.

Correlated effects on haltere shapes: The halteres of LLH and LLL flies were compared in five linear dimensions (Figure 8 and Table 9). This comparison is not as sensitive to shape differences as comparisons of angular offsets from control baselines would be. This method was used because of the extreme difficulty of obtaining accurate haltere measurements, as it elimi-

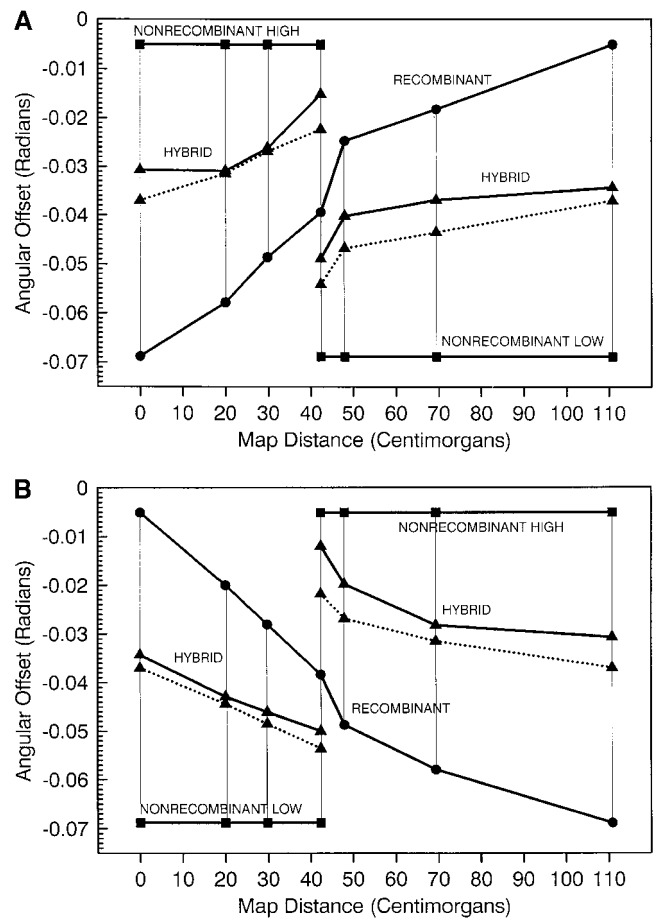


Figure 7.—Phenotypes of nonrecombinant lines (■, horizontal), representative single-crossover lines (●, long diagonals), and their hybrids (▲, short solid diagonals). Vertical lines connect parents and offspring. Dotted lines below hybrid phenotypes show the midpoints between parental phenotypes for each cross. All hybrids between recombinant and nonrecombinant lines show nearly additive action of alleles in heterozygous parts of the chromosome. (A) Hybrids of H-L recombinants. (B) Hybrids of L-H recombinants.

TABLE 8
Leg and wing shape effects of the whole third chromosome

	Line LLH		Line LLL		A (LLH-LLL)	B (base SD)	A/B
	Mean	±SD	Mean	±SD			
Prothoracic femur	-0.0180	±0.0155	+0.0053	±0.0123 ***	-0.0233	0.0153	1.52
Prothoracic tibia	+0.0058	±0.0225	-0.0178	±0.0163 ***	+0.0236	0.0177	1.33
Mesothoracic femur	-0.0293	±0.0158	-0.0122	±0.0163 ***	-0.0171	0.0178	0.96
Mesothoracic tibia	+0.0275	±0.0204	-0.0026	±0.0184 ***	+0.0301	0.0206	1.46
Metathoracic femur	-0.0114	±0.0133	+0.0126	±0.0164 ***	-0.0240	0.0195	1.23
Metathoracic tibia	+0.0167	±0.0173	-0.0051	±0.0168 ***	+0.0218	0.0179	1.22
Wing (index <i>F</i>)	-0.0073		-0.0689		+0.0616	0.0063	9.78

Leg-segment shapes in angular offsets from control population allometric baselines.

D_1 is the width of segment at widest point; D_2 is the width of the same segment at narrowest proximal part. Sample size is 100 males for each mean. ***, $P < 10^{-6}$. Wing-shape values from means of nonrecombinant lines are included for comparison. |A/B| gives the absolute value of third-chromosome shape effects in standard deviations of the wild-type control population for each trait (*cf.* Table 1).

nated the need to measure a large sample of control halteres to create the baseline (see materials and methods). No significant differences in haltere dimensions were found between lines LLH and LLL. The statistical power of each comparison was estimated by the formula $z_{\text{power}} = \Delta_H / \text{SED} - t$, where Δ_H is the hypothetical difference of 5 μm , SED is the standard error of the difference in means, $t_{0.05} = 1.984$ for d.f. = 98, and z_{power} has been tabulated with the corresponding values of statistical power (Motulsky 1995, p. 215). Halteres, though serially homologous to wings, show no detectable correlated effects of the wing-shape alleles that differ on the H and L third chromosomes.

DISCUSSION

The genetic control of wing shape in *D. melanogaster* involves many loci with small effects. These loci recombine readily due to their dispersion along the chromosomes; they segregate at intermediate frequencies in wild populations; their effects are mostly additive; and they have generally only minor pleiotropic effects on other aspects of body form or on reproductive fitness.

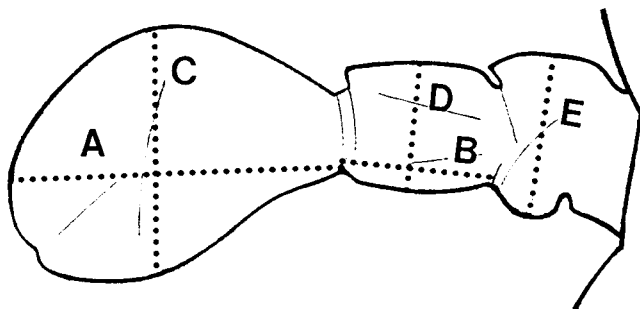


Figure 8.—Outline of left haltere, dorsal aspect, anterior side at top. Measurements of dimensions A–E are shown in Table 9.

These facts were inferred from quantitative studies of natural variation, selection response, and inbreeding effects on shape (Weber 1990, 1992) that preceded this study. The present results confirm several of these features and add some details, in particular for one shape trait on one chromosome. There are also important questions that remain unresolved.

Unlimited polygenes vs. QTL: Statistical analyses of QTL have certain inherent ambiguities. Effects are explained with the smallest defensible number of QTL, and often only QTL with larger effects may be interesting. However, any factor identified by these methods may actually represent a cluster of loci. Thus there is always the potential for an undercount of the true number of loci, especially when statistically supported QTL are many and dense. It is also clear that multiple alternative sets of QTL effects can be derived to account for the same genetic variance. The possible ways to do this tend to mount as the number of QTL increases. These facts should motivate an interest in supplemental ways of looking at effects.

If markers are dense enough to eliminate hidden double crossovers between them, then the H or L character of any interval between markers is only ambiguous if it spans a detected crossover. Therefore the genotypes of single recombinants are known with greater accuracy than the genotypes of double or triple recombinants. If single-recombinant lines are numerous, the graphs of their grand means vs. their breakpoints provide a robust picture of mean effects. Stepwise changes show the locations and magnitudes of effects. Significantly nonmonotonic points are reasonably interpreted as recombination linkage.

The reciprocal profiles of HL and LH single recombinants check each other (Figure 3A). Matching increments, of equal magnitude in both profiles, indicate genetic effects that are the same in different combinations, *i.e.*, not interacting with other loci on the chromo-

TABLE 9
Haltere dimensions

Dimension	Line LLH		Line LLL		<i>P</i>	Power (%)
	Length (mm)	±SD	Length (mm)	±SD		
A	0.179	±0.010	0.183	±0.010	NS	71
B	0.074	±0.009	0.074	±0.009	NS	77
C	0.112	±0.005	0.115	±0.007	NS	98
D	0.060	±0.005	0.060	±0.004	NS	100
E	0.079	±0.004	0.078	±0.003	NS	100

Haltere dimensions shown in Figure 8 compared between high and low third-chromosome lines. Means ±SD of samples of 50 male flies. NS, no dimensions were significantly different. Power of individual *t*-tests estimated to nearest whole percentage for $P \leq 0.05$ and difference of 0.005.

some. Unequal increments, which separate parts of the profiles when one is inverted on the other, indicate genetic interactions. Simple pairwise interactions should stand out because one recombination between the two loci turns the effect on or off. This separates the profiles between the loci by a distance equal to the interactive effect. The type of interaction can be partly worked out from the direction of the split.

Figure 3A can be contrasted with Figure 4 of Shrimpton and Robertson (1988), showing similar plots of single-recombinant lines that were used to map loci for sternopleural bristle number in *D. melanogaster* on the third chromosome. In that case, the plots do not have matching profiles, revealing prominent interactions among genes on the right arm. In other systems, QTL have shown various amounts of interaction. A recent study of QTL for abdominal and sternopleural bristle number (Long *et al.* 1995) found significant epistasis in both traits. A review by Tanksley (1993) reports that strong interactions among QTL are not common. However, the resolution achievable in QTL studies is usually not high enough to exclude interactions within complexes of tightly linked loci (Cabot *et al.* 1994; Palopoli and Wu 1994), which would behave like independent factors in a typical QTL study.

The graphic analysis of chromosome 3 presented here avoids any attempt to enumerate or characterize loci. The underlying model assumes large numbers of polygenes, whose effects approximate a continuous but not linear function of chromosome length. The other assumption is that there are no interactions, so that any segment of the chromosome has the same effect in any combination. Thus the small net interactions revealed along the chromosome in Figure 3C are averaged out as if they were only error among line means. The resulting predictions explain most of the variation ($R^2 = 0.93$).

Independent analysis by MIM confirms that many subequal additive effects are present. Another result is that important interactions may exist that cannot be resolved by the graphic analysis. Out of the 11 QTL, all but one (QTL 7) have at least one significant pairwise

interaction. The two largest interactions (0.0138 and 0.0129) are larger than the largest main effect (0.0115). The sum of absolute magnitudes of the nine detected pairwise interactions is 98% as large as the sum of main effects. However, interactions are approximately bal-

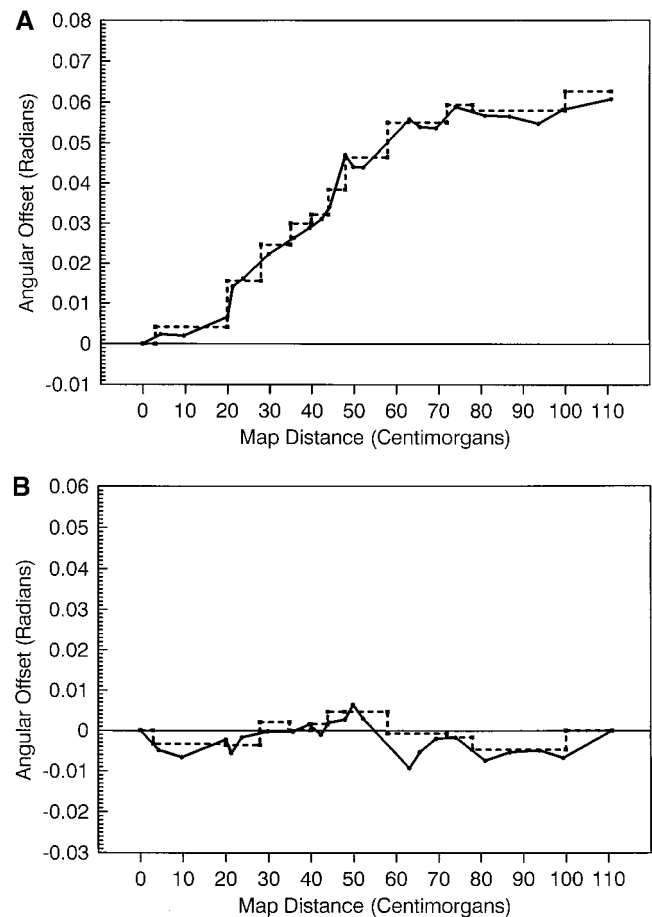


Figure 9.—Comparison of continuous effects from graphic analysis of single recombinants (solid lines) with point effects estimated by multiple interval mapping analysis (dashed lines). (A) Cumulative mean effects from Figure 3B and cumulative main effects from Table 5. (B) Net interactive effects from Figure 3C and Table 5.

anced between positive and negative effects. These balanced interactions occur in QTL pairs that span nearly the same regions, so that their effects are also geometrically balanced along the chromosome. This symmetry is revealed by the four largest pairwise interactions from Table 5:

$$\text{QTL 3} + \text{QTL 9} \dots + 0.0138$$

$$\text{QTL 5} + \text{QTL 9} \dots - 0.0129$$

$$\text{QTL 3} + \text{QTL 8} \dots - 0.0081$$

$$\text{QTL 5} + \text{QTL 8} \dots + 0.0088.$$

Each pair is nearly symmetrical with another that has opposite effects. Therefore when effects are added sequentially as in Figure 3A, interactions largely cancel out in both directions. Otherwise, large vertical separations would appear between the profiles of HL and LH single-recombinant means.

The main effects of the 11 QTL from Table 5 give a good fit to the graph of cumulative effects based on single recombinants (Figure 9A). The interactions among QTL also match the graph of net interactions based on single recombinants (Figure 9B). The graphic and statistical analyses were done independently by K.W. and Z.B.Z., except that QTL 10 with its marginal LOD score was accepted into the QTL model because of K.W.'s insistence that the single recombinants show repulsion linkage in that region, implying the existence of an effect. Otherwise the two ways of looking at the data were developed entirely separately. The close fit between them in Figure 9, A and B, was only noted afterward.

The simple graphic analysis and the complex statistical one are in general agreement. Whether effects are concentrated into the minimum possible number of sites (~ 11) or divided among some larger number, their number is large, their effects are subequal, and their distribution is diffuse and proportionate to Figure 3B. The complexity of the data is apparent in the attempts to evaluate interactions. In the QTL analysis, interactions are seen to be nearly as large as main effects (though with generally lower LOD scores). Among interacting QTL pairs, symmetries of location, magnitude, and sign appear to reduce large interactions to small net effects along the chromosome. The predominance of negative interactions could be explained most simply by frequent redundancies among loci that act by similar mechanisms; but this might not accord with the generally additive action of alleles in heterozygotes.

In any case, when all is said and done, we must admit that we are still left with the basic questions of quantitative genetics. Exactly how many genes are there, where are they, and what are their individual effects?

Advantages and limitations of MIM: Compared with other current QTL mapping methods, MIM has several advantages including increased statistical power and res-

olution (Kao *et al.* 1999). MIM also provides appropriate estimation of individual QTL effects (including epistatic effects) and their contribution to variances and covariances.

However, it must be noted that the estimation of genetic parameters and interpretation of mapping results depend critically on model selection. Model selection in a high and unknown dimension is very complicated and difficult, particularly when it is based on genetic map positions, not just on markers. There could be numerous peaks separated by valleys or connected by ridges in a likelihood landscape with different dimensions. Any model selected, including the current one, may well be just a local peak, and there is no guarantee that a global peak can be found. It is possible that the number of effect components is underestimated; that is to say, that the 20 effects estimated here could be composed of more underlying biological components.

Not all estimates of QTL positions are sensitive to model selection. Some QTL position estimates are relatively consistent in different analyses and competing models and are largely independent of estimates of positions of other QTL and epistatic components. Other QTL estimates are, however, very sensitive to model selection and estimates of other QTL parameters. Among the 11 QTL mapped, position estimates of 8 (QTL 1, 2, and 6–11) are very consistent and relatively independent of mapping of other QTL and selection of epistatic components. These positions are consistently picked up in different analyses and in different models. Position estimates of QTL 3, 4, and 5 are, however, somewhat sensitive to model selection; *i.e.*, estimates may shift locally if some other QTL effects are added to or dropped from the model.

The nature of wing-shape genes: The loci of *D. melanogaster* listed by Lindsley and Zimm (1992) include many with major effects on the wing or with visible pleiotropic effects on the wing. Perhaps other alleles at such loci have small quantitative effects like those detected here (see Falconer and Mackay 1996). It seems unlikely that a class of genes as numerous as wing-shape genes appear to be, in this and previous studies (Weber 1990, 1992), would not include any known loci. On the other hand, it will also be rather amazing if the detailed sculpting of the wing is achieved just by tuning the regulation of mostly known genes that often act over broad areas and in different domains during development. This would apply especially to the complex base (Weber 1992) and hinge regions. It remains to be seen whether any wing-shape polygenes will turn out to be familiar loci.

Thanks to Trudy Mackay for explaining the method, to Cathy Laurie and Tony Long for advice, to Lynn Stam for teaching *in situ* labeling, to Burke Judd and Karl Suter for providing *roo*, and to Brian Charlesworth and Stavroula Assimacopoulos for the transposable elements 412 and 297. Thanks also to Andy Clark and two anonymous reviewers

for suggestions on the manuscript. This work was supported by a grant from the National Science Foundation (DEB-9407005) to K.W. and by U.S. Public Health Service grant GM-45344 to Z.-B.Z.

LITERATURE CITED

- Abramowitz, M., and I. A. Stegun, 1970 *Handbook of Mathematical Functions*. Dover, New York.
- Ashburner, M., 1989 *Drosophila: A Laboratory Handbook*. Cold Spring Harbor Laboratory Press, Cold Spring Harbor, NY.
- Basten, C., B. S. Weir and Z.-B. Zeng, 1998 *QTL Cartographer: A Reference Manual and Tutorial for QTL Mapping*. Department of Statistics, North Carolina State University, Raleigh, NC.
- Cabot, E. L., A. W. Davis, N. A. Johnson and C.-I. Wu, 1994 Genetics of reproductive isolation in the *Drosophila simulans* clade: complex epistasis underlying hybrid male sterility. *Genetics* **137**: 175–189.
- Churchill, G. A., and R. W. Doerge, 1994 Empirical threshold values for quantitative trait mapping. *Genetics* **138**: 963–971.
- Cowley, D. E., and W. R. Atchley, 1988 Quantitative genetics of *Drosophila melanogaster*. II. Heritabilities and genetic correlations between sexes for head and thorax traits. *Genetics* **119**: 421–433.
- Cowley, D. E., W. R. Atchley and J. J. Rutledge, 1986 Quantitative genetics of *Drosophila melanogaster*. I. Sexual dimorphism in genetic parameters for wing traits. *Genetics* **114**: 549–566.
- Falconer, D. S., and T. F. C. Mackay, 1996 *Introduction to Quantitative Genetics*. Longman, Harlow, Essex, United Kingdom.
- Hartl, D. L., and E. R. Lozovskaya, 1995 *The Drosophila Genome Map: A Practical Guide*. R. G. Landes Co., Austin, TX.
- Kao, C.-H., and Z. B. Zeng, 1997 General formulae for obtaining the MLEs and the asymptotic variance-covariance matrix in mapping quantitative trait loci when using the EM algorithm. *Biometrics* **53**: 653–665.
- Kao, C.-H., Z.-B. Zeng and R. Teasdale, 1999 Multiple interval mapping for quantitative trait loci. *Genetics* **152**: 1203–1216.
- Lindsley, D. L., and G. G. Zimm, 1992 *The Genome of Drosophila melanogaster*. Academic Press, San Diego.
- Long, A. D., S. L. Mullaney, L. A. Reid, J. D. Fry, C. H. Langley *et al.*, 1995 High resolution mapping of genetic factors affecting abdominal bristle number in *Drosophila melanogaster*. *Genetics* **139**: 1273–1291.
- Motulsky, H., 1995 *Intuitive Biostatistics*. Oxford University Press, Oxford.
- Nuzhdin, S. V., E. G. Pasyukova, C. L. Dilda, Z.-B. Zeng and T. F. C. Mackay, 1997 Sex-specific quantitative trait loci affecting longevity in *Drosophila melanogaster*. *Proc. Natl. Acad. Sci. USA* **94**: 9734–9739.
- Palopoli, M. F., and C.-I. Wu, 1994 Genetics of hybrid male sterility between *Drosophila* sibling species: a complex web of epistasis is revealed in interspecific studies. *Genetics* **138**: 329–341.
- Scherer, G., C. Tschudi, J. Perera, H. Delius and V. Pirrotta, 1982 B104, a new dispersed repeated gene family in *Drosophila melanogaster* and its analogies with retroviruses. *J. Mol. Biol.* **157**: 435–451.
- Shrimpton, A. E., and A. Robertson, 1988 The isolation of polygenic factors controlling bristle score in *Drosophila melanogaster*. I. Allocation of third chromosome sternopleural bristle effects to chromosome sections. *Genetics* **118**: 437–443.
- Sokal, R. R., and F. J. Rohlf, 1969 *Biometry*. Freeman, San Francisco.
- Tanksley, S. D., 1993 Mapping polygenes. *Annu. Rev. Genet.* **27**: 205–233.
- Weber, K. E., 1988 A system for rapid morphometry of whole, live flies. *Dros. Inf. Serv.* **67**: 97–102.
- Weber, K. E., 1990 Selection on wing allometry in *Drosophila melanogaster*. *Genetics* **126**: 975–989.
- Weber, K. E., 1992 How small are the smallest selectable domains of form? *Genetics* **130**: 345–353.
- Zeng, Z.-B., 1994 Precision mapping of quantitative trait loci. *Genetics* **136**: 1457–1468.

Communicating editor: A. G. Clark